ISSN 1674-1056
http://cpb.iphy.ac.cn
http://iopscience.iop.org/cpb
中国物理 B
Chinese Physics
中国物理
Chinese Physics B

One-dimensional structure made of periodic slabs of SiO_2/InSb offering tunable wide band gap at terahertz frequency range

Sepehr Razi[1], Fatemeh Ghasemi[2]

Citation: Chin. Phys. B . 2019, 28(12): 124205 . **doi:** 10.1088/1674-1056/ab4d46
Journal homepage: http://cpb.iphy.ac.cn; http://iopscience.iop.org/cpb

What follows is a list of articles you may be interested in

Numerical investigation on coherent mid-infrared supercontinuum generation in chalcogenide PCFs with near-zero flattened all-normal dispersion profiles

Jie Han(韩杰), Sheng-Dong Chang(常圣东), Yan-Jia Lyu(吕彦佳), Yong Liu(刘永)
Chin. Phys. B . 2019, 28(10): 104204 . **doi:** 10.1088/1674-1056/ab3f25

Comment on “Band gaps structure and semi-Dirac point of two-dimensional function photonic crystals” by Si-Qi Zhang *et al.*

Hai-Feng Zhang(章海锋)
Chin. Phys. B . 2018, 27(1): 014205 . **doi:** 10.1088/1674-1056/27/1/014205

Dynamically controlled optical nonreciprocity of a double-ladder system with spontaneously generated coherence in moving atomic optical lattice

Nuo Ba(巴诺), Xiang-Yao Wu(吴向尧), Dong-Fei Li(李东飞), Dan Wang(王丹), Jin-You Fei(费金有), Lei Wang(王磊)
Chin. Phys. B . 2017, 26(5): 054207 . **doi:** 10.1088/1674-1056/26/5/054207

Extreme narrow photonic passbands generated from defective two-segment-connected triangular waveguide networks

Tang Zhen-Xing, Yang Xiang-Bo, Lu Jian, Liu Timon Cheng-Yi
Chin. Phys. B . 2014, 23(4): 044207 . **doi:** 10.1088/1674-1056/23/4/044207

Characteristics of photonic bands generated by quadrangular multiconnected networks

Luo Rui-Fang, Yang Xiang-Bo, Lu Jian, Liu Timon Cheng-Yi
Chin. Phys. B . 2013, 22(10): 104211 . **doi:** 10.1088/1674-1056/22/10/104211

One-dimensional structure made of periodic slabs of SiO_2/InSb offering tunable wide band gap at terahertz frequency range

Sepehr Razi[1,†] and Fatemeh Ghasemi[2]

[1] Faculty of Electrical Engineering, Urmia University of Technology (UUT), Urmia, Iran
[2] Department of Energy Engineering and Physics, Amirkabir University of Technology, PO Box 15875-4413, Tehran, Iran

(Received 17 May 2019; revised manuscript received 4 September 2019; published online 15 November 2019)

Optical features of a semiconductor–dielectric photonic crystal are studied theoretically. Alternating layers of micrometer sized SiO_2/InSb slabs are considered as building blocks of the proposed ideal crystal. By inserting additional layers and disrupting the regularity, two more defective crystals are also proposed. Photonic band structure of the ideal crystal and its dependence on the structural parameters are explored at the first step. Transmittance of the defective crystals and its changes with the thicknesses of the layers are studied. After extracting the optimum values for the thicknesses of the unit cells of the crystals, the optical response of the proposed structures at different temperatures and incident angles are investigated. Changes of the defect layers' induced mode(s) are discussed by taking into consideration of the temperature dependence of the InSb layer permittivity. The results clearly reflect the high potential of the proposed crystals to be used at high temperature terahertz technology as a promising alternative to their electronic counterparts.

Keywords: photonic band gap, photonic crystal, semiconductor layer, defect mode

PACS: 42.70.Qs, 78.67.Pt **DOI:** 10.1088/1674-1056/ab4d46

1. Introduction

Nowadays we are witnessing increasing progresses in different branches of the laser and photonic technologies which are pointing towards the rapid transitions from pure science to experiments.[1–5] However, these successes are not just related to the advancements in the fabrication techniques alone. Foundation of new materials and suggestions of more applicable elements have become very influential in these regards. Photonic crystals (PCs) are undoubtedly one of the structures that many advancements could be related to. The idea of using two/more dielectrics stacked periodically in one, two, or three dimensions for manipulation of the electromagnetic waves propagation is not a new idea.[5–7] There exist numerous reports in which optical features of various kinds of these structures have been investigated.[8–13] They have been widely proposed in fabrications of not only light sources such as lasers/diodes[14,15] but also detectors and transducers,[15] all optical filters, mirrors, and switches.[16–26] Nevertheless, these structures are still on tops of attention for new photonic elements design due to their unique characteristics. Valuable experimental techniques including chemical/optical methods and various deposition approaches are also suggested for their fabrication.[24,25] Laser technology has been also applied in this regards following its great successes in material surface patterning.[26,27]

Needs for tunable components in new generations of optical integrated circuits (OICs) reflect the importance of the PCs even more evident. This has been an important issue over the last few years for researchers and manufacturers of photonic technology. Different structures have been suggested in this regards by benefiting the temperature dependence of the refractive index of a specific material,[28] crystals with electro/magneto optical features,[29] or using some materials with efficient response to external mechanical tensions.[30] One could also refer to the valuable Refs. [30]–[37] for other novel structures with applications in the visible–infrared range.

In the light of these valuable reports, here in this paper we propose new structures with interesting optical responses in terahertz (THz) frequency range. The suggested crystals have some advantages such as using layers of well-known SiO_2 and InSb materials with reasonable thicknesses and having sensible numbers of periods which are very vital from experimental points of view. Thus, it seems that their fabrication is completely possible in reality. The paper is organized as follow: the mathematical approaches are introduced at first. The one-dimensional (1D) ideal crystal composed of periodic layers of SiO_2 and InSb is presented next and then its optical features are explored comprehensively. Special attention is paid to the dependence of the photonic band gap (PBG) on the layers' thickness. In addition, selecting the optimum widths, two different defective structures are considered and the induced variations in the PBG and transmission spectrum are studied. Then, tunability of the optical features of the structures is extensively investigated by taking into consideration of the crystal thermal response. The results are discussed by focusing on the well-known physical facts. At last, the dependence of the proposed crystals' transmittance on the wave incident angle is explored.

†Corresponding author. E-mail: s.razi@uut.ac.ir

© 2019 Chinese Physical Society and IOP Publishing Ltd

2. Methods and materials

2.1. Wave propagation and reflection from interfaces

The incident plane wave on the interface of two isotropic media splits into two parts (reflected and transmitted waves). The incident (i), transmitted (t), and reflected (r) plane waves can be defined as

$$\boldsymbol{E}_{\mathrm{i,t,r}} = \mathrm{Re}\left\{\boldsymbol{E}_{\mathrm{ei,t,r}} \exp[\mathrm{j}(\omega t - \boldsymbol{k}_{\mathrm{i,t,r}} \cdot \boldsymbol{R})]\right\}, \tag{1}$$

where $\boldsymbol{E}_{\mathrm{ei,t,r}}$ and $\boldsymbol{k}_{\mathrm{i,t,r}}$ denote the complex envelopes and wave vectors, respectively. At the interface, due to the boundary conditions, we have

$$(\boldsymbol{k}_i \cdot \boldsymbol{R})|_{z=0} = (\boldsymbol{k}_{\mathrm{r}} \cdot \boldsymbol{R})|_{z=0} = (\boldsymbol{k}_{\mathrm{t}} \cdot \boldsymbol{R})|_{z=0}. \tag{2}$$

For a slab of dielectric/semiconductor, there exist other field components $(\boldsymbol{E}'_{\mathrm{r}}, \boldsymbol{H}'_{\mathrm{r}})$ which are the reflections from the second interface. Then the total phasor of the electric field can be written as

$$\boldsymbol{E}_{\mathrm{p}} = \begin{cases} \boldsymbol{E}_{\mathrm{i}} \mathrm{e}^{-\mathrm{j}\boldsymbol{k}_{\mathrm{i}} \cdot \boldsymbol{R}} + \boldsymbol{E}_{\mathrm{r}} \mathrm{e}^{-\mathrm{j}\boldsymbol{k}_{\mathrm{r}} \cdot \boldsymbol{R}}, & z < 0, \\ \boldsymbol{E}_{\mathrm{t}} \mathrm{e}^{-\mathrm{j}\boldsymbol{k}_{\mathrm{t}} \cdot \boldsymbol{R}} + \boldsymbol{E}'_{\mathrm{r}} \mathrm{e}^{-\mathrm{j}\boldsymbol{k}'_{\mathrm{r}} \cdot \boldsymbol{R}}, & z > 0. \end{cases} \tag{3}$$

The magnetic field phasor is calculated by using the Maxwell's equations[34] $\boldsymbol{H}_{\mathrm{p}} = -\mathrm{j}(\mu\omega)^{-1}\nabla \times \boldsymbol{E}_{\mathrm{p}}$. According to the boundary conditions, all tangential components of the electric and magnetic fields must be continuous. Thus for a TE polarized wave, we have

$$\begin{aligned} & \boldsymbol{E}_{\mathrm{i,TE}} + \boldsymbol{E}_{\mathrm{r,TE}} \\ = \; & \boldsymbol{E}_{\mathrm{t,TE}} + \boldsymbol{E}'_{\mathrm{r,TE}}, \sqrt{\frac{\varepsilon_1}{\mu_1}}(\boldsymbol{E}_{\mathrm{i,TE}} + \boldsymbol{E}_{\mathrm{r,TE}})\cos\theta_1 \\ = \; & \sqrt{\frac{\varepsilon_2}{\mu_2}}(\boldsymbol{E}_{\mathrm{t,TE}} + \boldsymbol{E}'_{\mathrm{r,TE}})\cos\theta_2. \end{aligned} \tag{4}$$

By using Eq. (4), the dynamical matrix of the TE wave is given by

$$\boldsymbol{D}(1)\begin{pmatrix} \boldsymbol{E}_{\mathrm{i,TE}} \\ \boldsymbol{E}_{\mathrm{r,TE}} \end{pmatrix} = \boldsymbol{D}(2)\begin{pmatrix} \boldsymbol{E}_{\mathrm{t,TE}} \\ \boldsymbol{E}'_{\mathrm{r,TE}} \end{pmatrix}, \tag{5}$$

where

$$\boldsymbol{D}(i) = \begin{pmatrix} 1 & 1 \\ \sqrt{\frac{\varepsilon_i}{\mu_i}}\cos\theta_i & -\sqrt{\frac{\varepsilon_i}{\mu_i}}\cos\theta_i \end{pmatrix}, \quad i = 1, 2. \tag{6}$$

As in the case of TE wave, according to the boundary conditions and considering the continuity of the tangential components and Maxwell's equations, the dynamical matrix of the TM wave is derived as

$$\boldsymbol{D}(i) = \begin{pmatrix} \cos\theta_i & \cos\theta_i \\ \sqrt{\frac{\varepsilon_i}{\mu_i}} & -\sqrt{\frac{\varepsilon_i}{\mu_i}} \end{pmatrix}, \quad i = 1, 2. \tag{7}$$

Furthermore, the propagation matrix is defined as[35]

$$\boldsymbol{P}_i = \begin{pmatrix} \mathrm{e}^{\mathrm{j}\phi_i} & 0 \\ 0 & \mathrm{e}^{-\mathrm{j}\phi_i} \end{pmatrix}, \tag{8}$$

where $\phi_i = k_0 n_i l_i \cos\theta_i$. Associating dynamical and propagation matrices for each layer of the stack, the electric and magnetic fields at two sides of the unit cell (SiO_2/InSb) could be related via a transfer matrix $M_{\mathrm{unitcell}} = D_{\mathrm{SiO_2}} P_{\mathrm{SiO_2}} D^{-1}_{\mathrm{SiO_2}} D_{\mathrm{InSb}} P_{\mathrm{InSb}} D^{-1}_{\mathrm{InSb}}$. Thus for the ideal structure with N periods of SiO_2/InSb layers, the total transfer matrix is given by

$$M = [D_{\mathrm{SiO_2}} P_{\mathrm{SiO_2}} D^{-1}_{\mathrm{SiO_2}} D_{\mathrm{InSb}} P_{\mathrm{InSb}} D^{-1}_{\mathrm{InSb}}]^N.$$

Similarly, for two proposed defective structures illustrated in Fig. 1, we have

$$\begin{aligned} M \; = \; & [D_{\mathrm{SiO_2}} P_{\mathrm{SiO_2}} D^{-1}_{\mathrm{SiO_2}} D_{\mathrm{InSb}} P_{\mathrm{InSb}} D^{-1}_{\mathrm{InSb}}]^{N_1} \\ & \times [D_{\mathrm{SiO_2}} P_{\mathrm{SiO_2}} D^{-1}_{\mathrm{SiO_2}}]^2 \\ & \times [D_{\mathrm{SiO_2}} P_{\mathrm{SiO_2}} D^{-1}_{\mathrm{SiO_2}} D_{\mathrm{InSb}} P_{\mathrm{InSb}} D^{-1}_{\mathrm{InSb}}]^{N_2}, \\ M \; = \; & [D_{\mathrm{SiO_2}} P_{\mathrm{SiO_2}} D^{-1}_{\mathrm{SiO_2}} D_{\mathrm{InSb}} P_{\mathrm{InSb}} D^{-1}_{\mathrm{InSb}}]^{N_1} \\ & \times [D_{\mathrm{InSb}} P_{\mathrm{InSb}} D^{-1}_{\mathrm{InSb}} D_{\mathrm{SiO_2}} P_{\mathrm{SiO_2}} D^{-1}_{\mathrm{SiO_2}}] \times \cdots \\ & \times [D_{\mathrm{SiO_2}} P_{\mathrm{SiO_2}} D^{-1}_{\mathrm{SiO_2}} D_{\mathrm{InSb}} P_{\mathrm{InSb}} D^{-1}_{\mathrm{InSb}}]^{N_2}. \end{aligned} \tag{9}$$

Extracting the elements of these matrices and implementing a MATLAB algorithm, reflection R, transmission T, and absorption A of the crystals can be calculated by[38,39]

$$R = |r|^2, \quad r = \frac{(m_{11} + m_{12}p_{n+1})p_0 - m_{21} - m_{22}p_{n+1}}{(m_{11} + m_{12}p_{n+1})p_0 + m_{21} + m_{22}p_{n+1}}, \tag{10}$$

$$T = \begin{cases} |t|^2, & (\mathrm{TE}), \\ \frac{p_0}{p_{n+1}}|t|^2, & (\mathrm{TM}), \end{cases}$$

$$t = \frac{2p_0}{(m_{11} + m_{12}p_{n+1})p_0 + m_{21} + m_{22}p_{n+1}}, \tag{11}$$

$$A = 1 - T - R. \tag{12}$$

Here p_0 is equal to $(\sqrt{\mu_0/\varepsilon_0})\cos(\theta_0)$ in the case of TE polarization and $(\sqrt{\mu_0/\varepsilon_0})/\cos(\theta_0)$ for TM. And p_{n+1} is $\sqrt{\mu_{n+1}/\varepsilon_{n+1}}\cos(\theta_{n+1})$ and $(\sqrt{\mu_{n+1}/\varepsilon_{n+1}})/\cos(\theta_{n+1})$ for TE and TM polarizations, respectively. Air is considered in our simulations as the surrounding input and output medium. ε_0 and ε_{N+1} denote the relative dielectric constants of the input and output planes, respectively.

2.2. Temperature dependence

Thermal fluctuations can lead to various linear/nonlinear optical and physical phenomena. Refractive index changes and material size variations are two famous effects in this regards. Thus it is necessary to include all these dependencies in the calculations to increase the accuracy of the simulations. The temperature dependence of the constituent layers' thicknesses due to the possible thermal expansions can be considered as[40]

$$l_i(T) = l_{i,0}(1 + \alpha\Delta T). \tag{13}$$

Here α and ΔT are respectively the thermal expansion coefficient and the temperature changes. Moreover, the thermo-optical effect of the temperature dependency of the refractive index is strongly related to the material structure. It has been proven that for gases, the refractive index always decreases as the temperature increases (at constant pressure). But for solid materials, the refractive index can either increase or decrease with temperature. It seriously depends on the internal structure of the material. The temperature dependence of the refractive index of each layer is given by[40]

$$n_i(T) = n_{i,0} + \beta\,\Delta T, \tag{14}$$

where β is the thermo-optic coefficient of the layer.

2.3. Thermo-optical features of InSb

Being as one of the main building blocks of the proposed PCs, before discussing the results, it is worth to review the thermo-optical features of the InSb semiconductor in more details. It has been proven that its relative permittivity is dependent on the temperature and frequency and can be described by the Drude model[38]

$$\begin{aligned}\varepsilon_{\rm D}(\omega,T) &= \varepsilon'_{\rm D}(\omega,T) - {\rm j}\varepsilon''_{\rm D}(\omega,T)\\ &= \varepsilon_\infty - \left\{\omega_{\rm p}^2/[\omega^2 - {\rm j}\omega\gamma(T)]\right\}\\ &= \varepsilon_\infty - \left\{\omega_{\rm p}^2/[\omega^2 + \gamma(T)^2]\right\}\\ &\quad - {\rm j}\left\{[\omega_{\rm p}^2\gamma(T)]/[\omega^3 + \omega\gamma(T)^2]\right\}.\end{aligned} \tag{15}$$

Here ε_∞ is the high frequency permittivity, $\gamma(T)$ is the damping factor, and $\omega_{\rm p}$ is the plasma frequency

$$\begin{aligned}&\omega_{\rm p} = 2\pi f_{\rm p} = \left(\frac{N(T)e^2}{\varepsilon_0 m^*}\right)^{1/2},\\ &N(T) = 5.76\times 10^{20} T^{3/2}\exp\left(-\frac{0.26}{2K_{\rm B}T}\right),\end{aligned} \tag{16}$$

where e, ε_0, m^*, and $K_{\rm B}$ are respectively the electron charge, permittivity of the vacuum, effective mass of the free carriers, and Boltzmann constant. T in this relation is in units of Kelvin and the intrinsic carrier density $N(T)$ is in units of $\rm m^{-3}$. It is clear that the plasma frequency of InSb depends strongly on the material temperature. Taking into considerations of the discussed permittivity (Eqs. (15) and (16)), the refractive index of InSb can be calculated by[38]

$$\tilde{n}_{\rm D} = \sqrt{\varepsilon_{\rm d}(\omega,T)} = n_{\rm d}(\omega,T) - {\rm j}k_{\rm d}(\omega,T). \tag{17}$$

The real part is the common refractive index and the imaginary part is the extinction coefficient.

3. Results and discussion

Figure 1 displays the schematics of the proposed 1D-PCs. All the layers are considered to be isotropic and the interfaces of the layers are parallel to the x–y plane. The z-axis is normal to the structure and N denotes the number of unit cells of the ideal crystal. N_1 and N_2 are the numbers of periods of the SiO_2/InSb layers without and with the defects. Two defective crystals, as shown in Fig. 1, are called the first defective PC (FDPC) and the second defective PC (SDPC) in the followings.

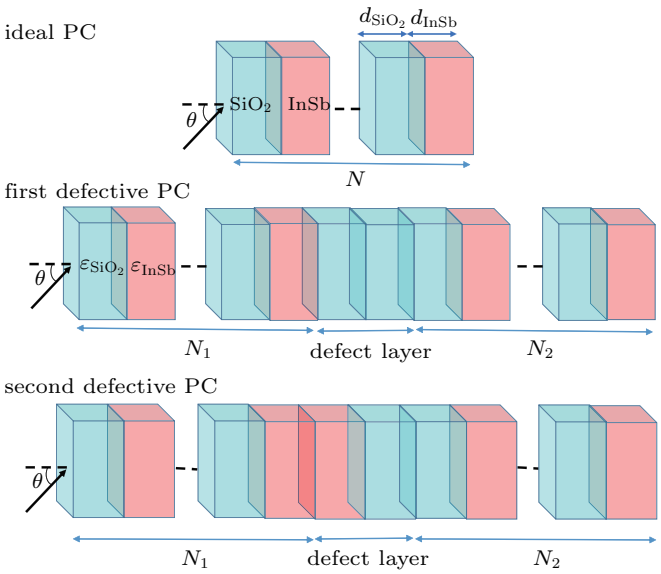


Fig. 1. Schematic illustration of the proposed 1D perfect (without any defects) and defective PCs based on SiO_2/InSb alternating layers. The incident angle is measured respect to the z-axis and $d_{\rm InSb}$ and d_{SiO_2} are the layers' thicknesses.

3.1. Ideal crystal

Dependence of the optical features of the ideal crystal (without any defect) on the thicknesses of the layers is studied at the first step. Numerical constants are taken as $\varepsilon_{SiO_2} = 2$, $d_{SiO_2} = 4$ μm, $d_{\rm InSb} = 4$ μm, $\alpha_{SiO_2} = 5.5\times 10^{-7}\ ^\circ{\rm C}^{-1}$, $\beta_{SiO_2} = 10^{-5}\ ^\circ{\rm C}^{-1}$, $m^* = 0.015m_0$, and $m_0 = 9.1\times 10^{-31}$ kg in the simulations. The photonic band structures of the crystal composed of 8 periods of SiO_2/InSb layers are presented in Fig. 2. Figure 2(a) corresponds to the dispersion curves of the crystals with various thicknesses of the SiO_2 layer (the InSb layer is 4 μm). Color maps of the wave vector versus frequency are also presented for various thicknesses of the layers to show the dependencies more clearly. It is seen that even at the lowest thickness of 2 μm, there are two PBGs at ∼ 6.8 THz to ∼ 8.5 THz and ∼ 13.6 THz to ∼ 16.6 THz frequency ranges. The numbers of the gaps at the thicknesses of 6 μm and 10 μm increase to 3 and 4, respectively. Figures 2(c) and 2(d) illustrate the dependencies on the thickness of the InSb layer (the SiO_2 layer is 4 μm). For an InSb layer of 2 μm thick, there exists a single wide PBG of ∼ 3.8 THz width. As the thickness increases, it shifts to the smaller wave vectors and its width decreases by about 47% at 4 μm. Interestingly, one more PBG is generated at the frequency range of ∼ 11.7 THZ to ∼ 13.8 THZ. Further increase in the thickness (thickness

of the InSb layer = 6 μm) results in the generation of three PBGs. Similarly, shifts towards the smaller wave vectors and reductions in the PBG widths are also observed. The trend of the changes is the same at the maximum selected thickness of 10 μm. Figures 2(e) and 2(f) present the changes of the PBGs when the thicknesses of both the layers are equally changed. For the layers with thicknesses of 2 μm, there exists one structural gap of ∼ 4.5 THz width with central frequency at 12.6 THz. Increasing the thicknesses of the layers to 4 μm, a new gap arises at the frequency interval of ∼ 5.5 THz to ∼ 7.5 THz. Further increasing the thicknesses of the layers results in red shift besides the appearance of new gap regions at higher frequencies. The widths of the gaps are also affected by the layers' thicknesses and smaller PBGs are observed for the structures with thicker layers.

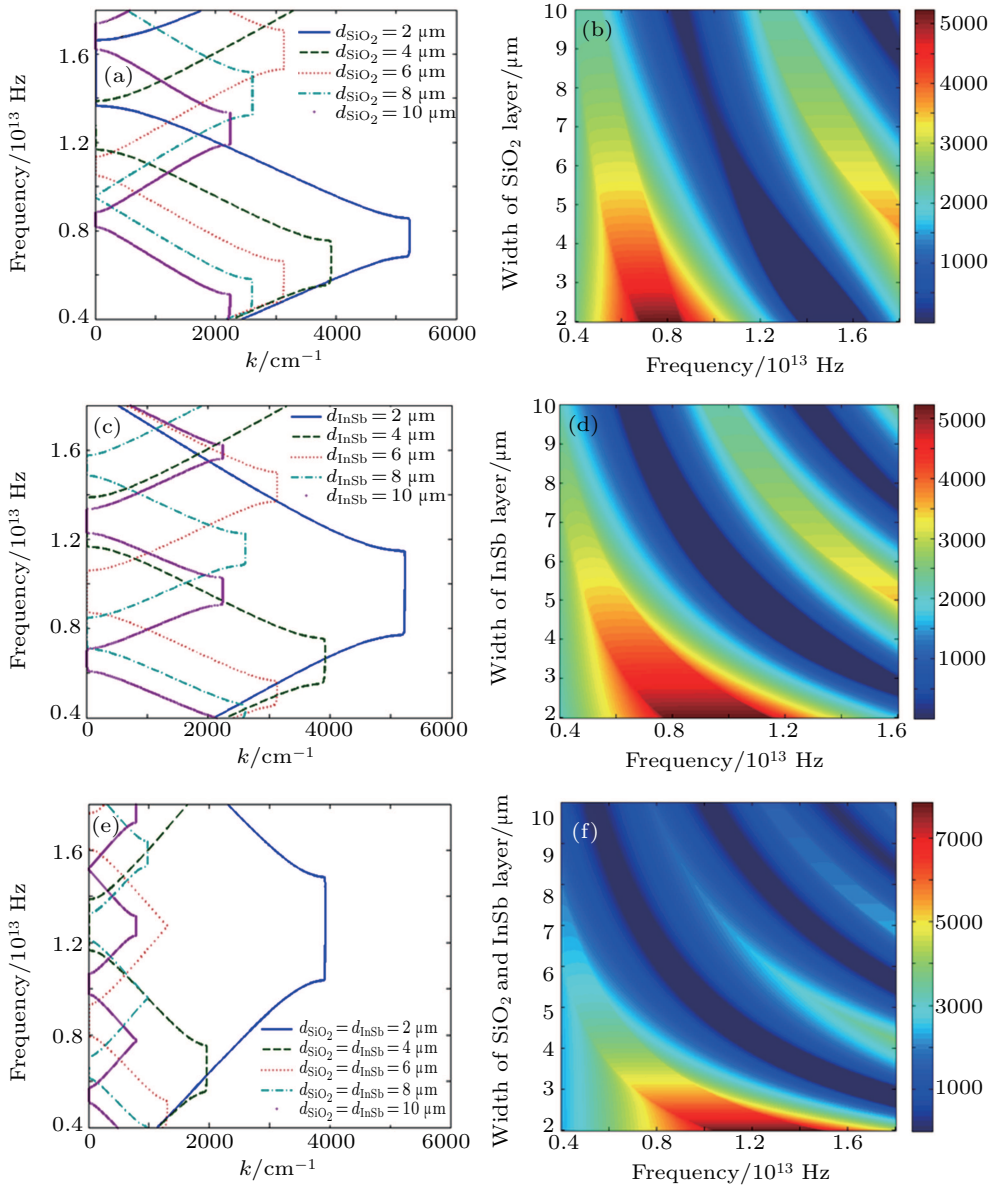


Fig. 2. Photonic band structure of the ideal perfect SiO_2/InSb PC. (a)–(d) The dependence of the dispersion on the SiO_2 and InSb layers' thicknesses. Panels (e) and (f) are for the structures having layers of equal thicknesses. Color maps represent the variations of the structure transmittance versus frequency and thickness of the layers. InSb and SiO_2 layers' thicknesses are 4 μm in (a), (b) and (c), (d), respectively. The crystal temperature is 300 K and the incidence angle is normal to the crystal in all cases.

3.2. Defective crystals

Transmittance spectra of the ideal crystal without any defect inside its structure and the first and second defective PCs are presented in Fig. 3. In all three spectra, there are two PBGs in the selected frequency range of 0.4–1.6 THz. But the widths of the gaps are not the same. No resonant peak exists inside the gaps of the ideal crystal. But in the cases of the first and second defective structures, there exist respectively one and two resonant modes in their PBGs. The second influence of the defect(s) insertion is the change in the PBGs width. It is clear that the smallest gaps belong to the ideal crystal and PBGs in the spectrum of the SDPC are wider than those in the spectrum

of the FDPC.

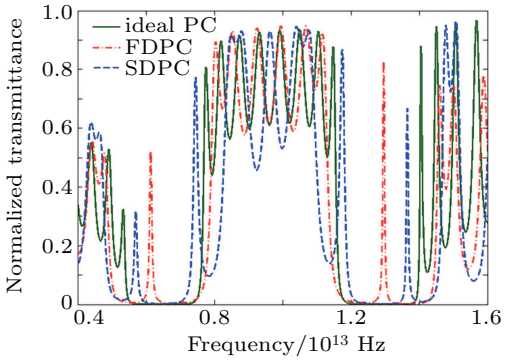


Fig. 3. Transmittance of TE polarized wave through the perfect crystal including 8 periods of SiO_2/InSb layers, and the FDPC and SDPC structures with $N_1 = 4$ and $N_2 = 3$. The thicknesses of the layers are 4 μm and the incident angle is normal to the crystal at $T = 300$ K.

For the FDPC, the intensity (height) of the mode in the second gap ($> 80\%$) is much higher than that in the first PBG ($< 60\%$). Similar relation is observed between the first and the third modes of the gaps in the spectrum of the SDPC (the numbering is from low to high frequencies). But the ratio of the second modes of the gaps is different and the 4th mode in the second gap has lower intensity than the 2nd one in the first PBG.

It is clear that the wide PBGs and the sharp resonant peaks of $\sim 100\%$ transmittance inside the gaps might find various applications in the fabrication of photonic devices such as optical filters, switches, wavelength samplers, etc. Thus the dependence of the optical features of the proposed crystals on the thicknesses of the layers is studied more systematically in order to find the optimum thicknesses for those applications.

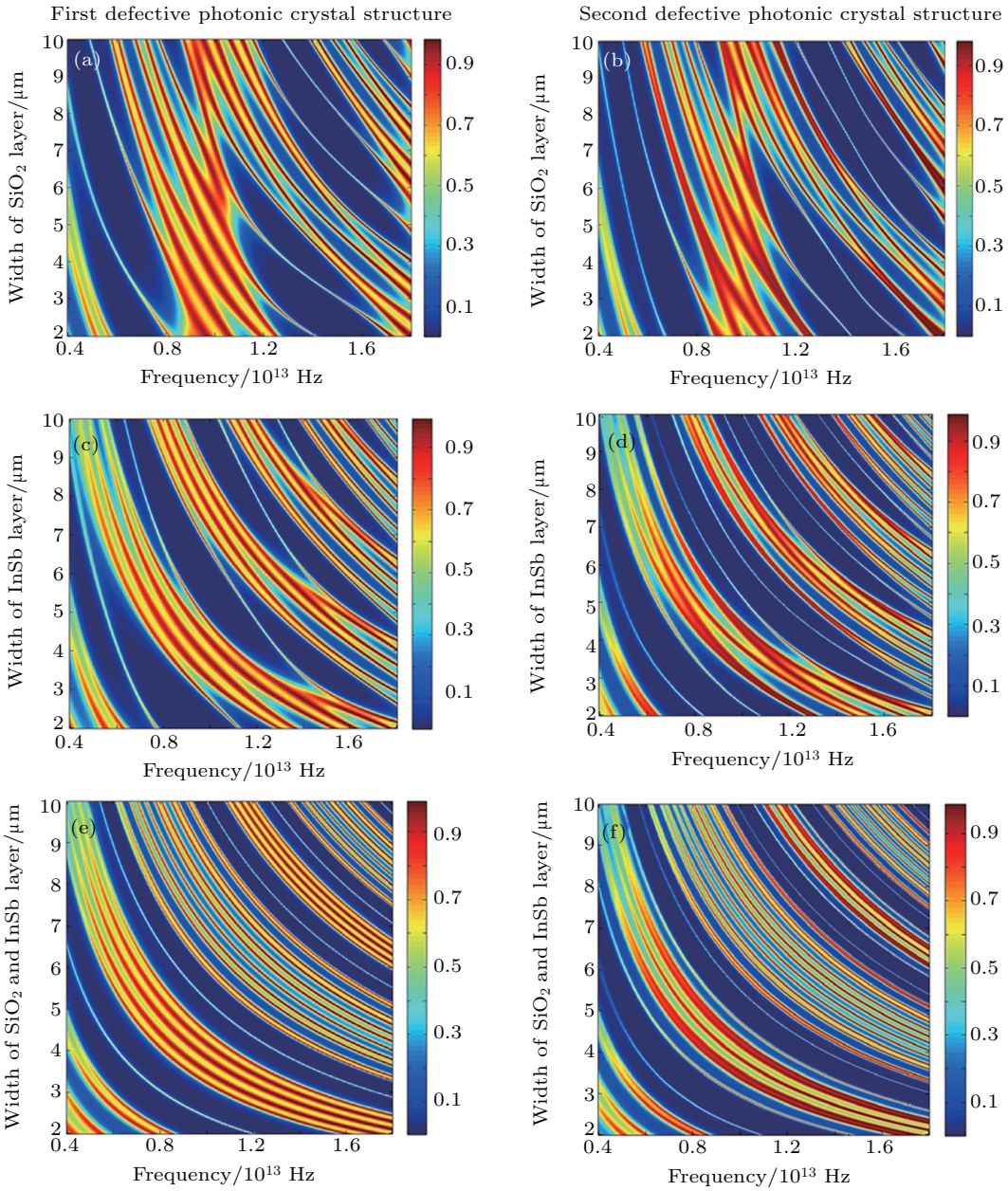


Fig. 4. Transmittance of a TE polarized wave as a function of frequency and layer thicknesses for the proposed SDPC and DDPC. InSb and SiO_2 layers' thicknesses are 4 μm in (a), (b) and (c), (d), respectively. The incident angle is normal to the crystal and the crystal temperature is assumed to be 300 K.

Figures 4(a)–4(f) illustrate the color maps of the transmittance versus frequency for different thicknesses of the SiO_2 and InSb layers. The graphs in the first column are for the FDPC and the ones in the second column belong to the SDPC. The dark regions are PBGs and the bright ones are the propagating bands. The results show that changing the thicknesses of the layers, not only the central frequency of the defect(s) induced resonant modes, but also both the PBG frequency intervals and the number of the gaps are changed. Compared to the InSb layer, dependencies to the SiO_2 layer thickness are more complicated for both the FDPC and SDPC structures. But when the layers have equal sizes, changes are more regular and predictable. The total PBG intervals experience red shifts with increasing thicknesses of the layers and the central frequency of the defect layer(s) induced resonant modes also shifts to the lower frequencies as a result. Interestingly, the width of the gaps and the location of the resonant mode(s) (its distances from the gap edges) remain constant with the thicknesses changed. However, the number of the PBGs increases with the increase of the layers' thicknesses.

3.3. Temperature dependence

Tunability of the optical features of the proposed crystals is studied in the next step. Figure 5 illustrates how seriously the transmittance through the FDPC depends on the crystal temperature. Increasing the crystal temperature, a general blue shift is observed on the whole spectrum. Figures 5(b) and 5(c) are the magnifications of the frequency ranges including the resonant modes. The result show that the first mode (peak in the first PBG) is more sensitive to the temperature than the second mode (peak in the second gap). As the temperature increases, both modes shift to higher frequencies and their intensities reduce. Alterations are clear for temperature changes of as small as 30 K. Transmittance as high as $\sim 60\%$ for the first mode and $\sim 90\%$ for the second mode is observed even at $T = 310$ K. Compared to some of the other proposed structures[39,41] which fail to respond well at high temperatures, this could be considered as a great advantage of the presented structure.

As the temperature increases, the whole transmittance spectrum of the SDPC blue shifts similar to what takes place for the SDPC. As a result, all the modes shift to higher frequencies with increasing temperature. The intensity (height) of the modes reduces. But the variations are not the same for all the modes. The first mode experiences the largest variations and the second and third ones show the lowest changes. It is worth noting once more that the numbering of the modes

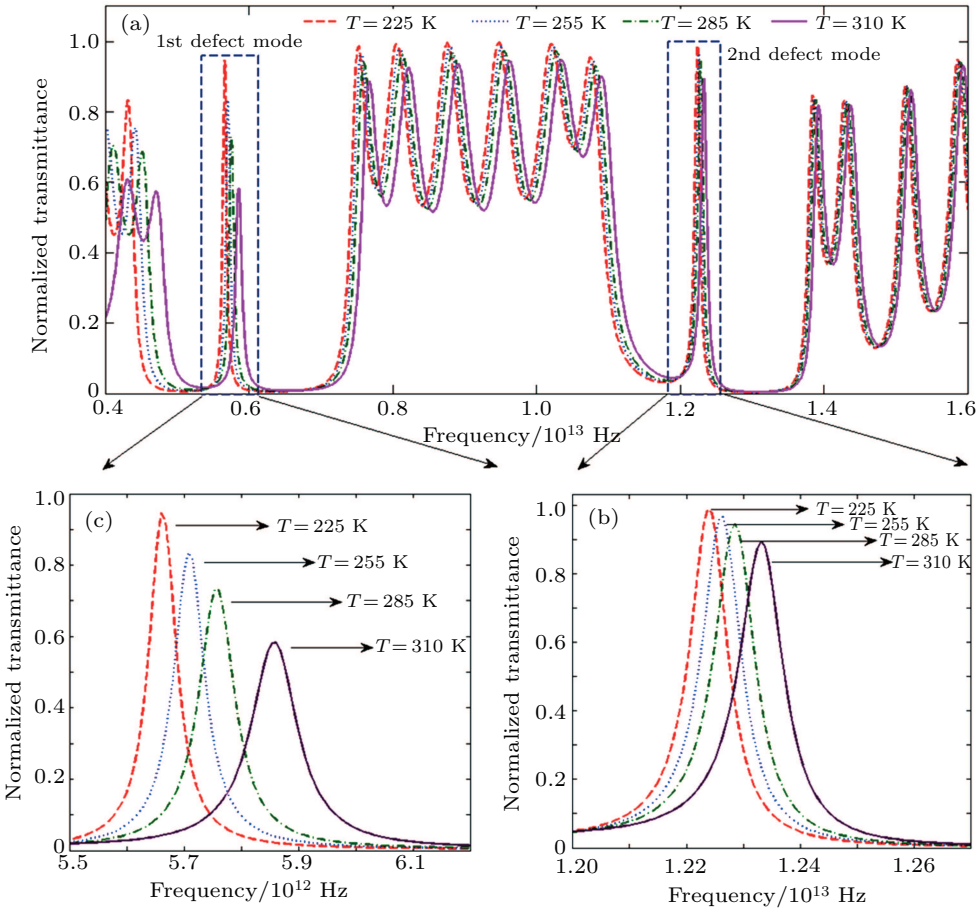


Fig. 5. Transmittance spectra of the single defect 1D-PC consisting of SiO_2/InSb alternating layers at different crystal temperatures of $T =$ 225 K, 255 K, 285 K, and 310 K. Panels (b) and (c) are the magnifications of the two PBG areas of the spectra. The incident angle is normal to the crystal and the thicknesses of the layers are 4 μm.

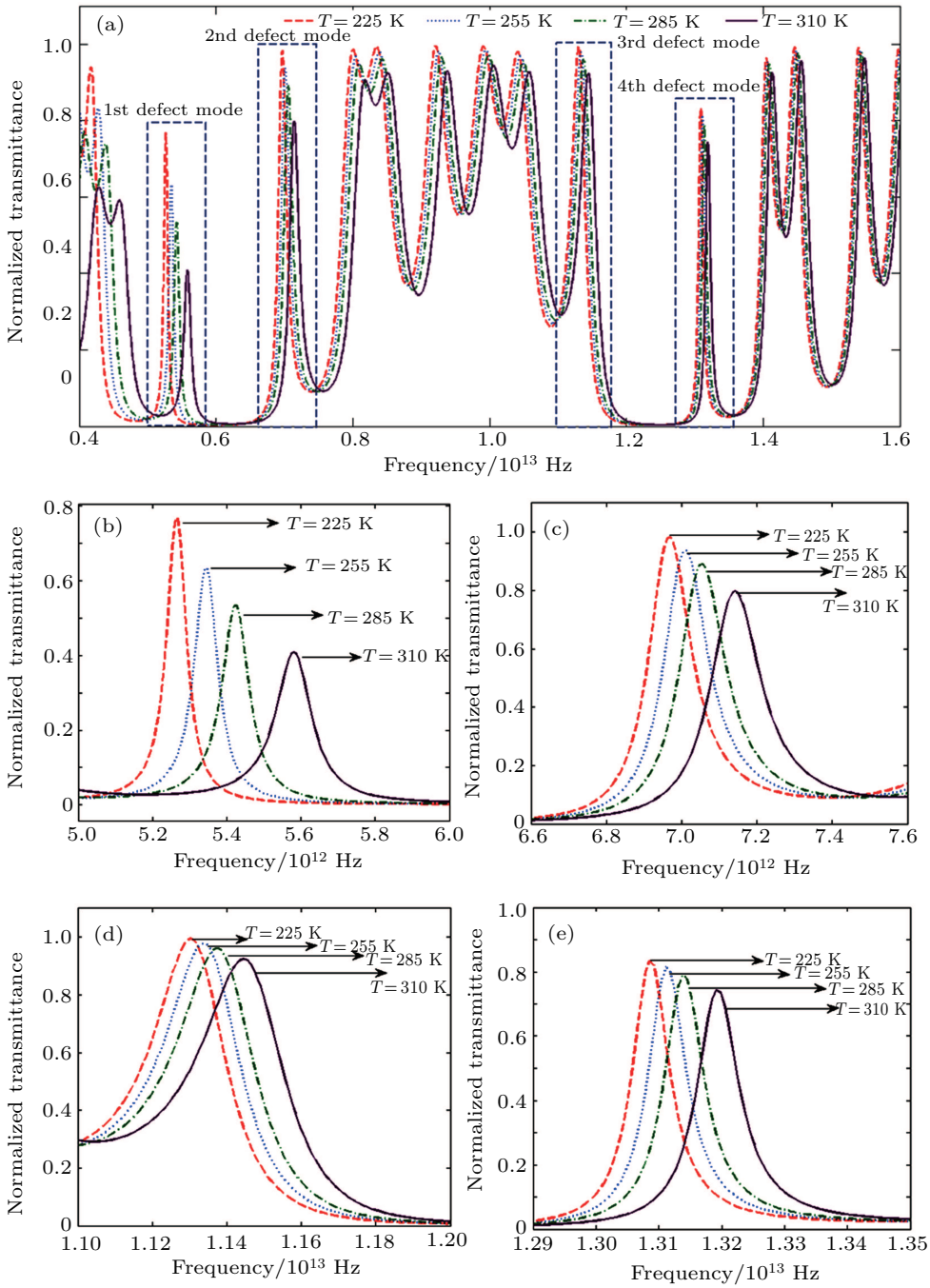


Fig. 6. Transmittance through SDPC for different crystal temperatures of $T = 225$ K, 255 K, 285 K, and 310 K. Panels (b)–(e) are respectively the magnifications of the frequency intervals containing the first up to the fourth resonant modes. The incident angle is normal to the crystal and the thicknesses of the layers are 4 μm.

is from left side of the spectrum to the right (lower frequencies to higher ones). Except the first mode with transmittance of $\sim 40\%$ at 310 K, all other modes have values higher than 70% even at room temperature. This reflects the potential of this structure and its successful performance at high temperatures without any need to cool the systems.

The interesting temperature dependence of the optical features might be related to the changes of the refractive index of the InSb layer with temperature. At terahertz frequency range, the refractive index of InSb is complex valued and temperature dependent as shown in Eqs. (15)–(17). Figure 7 shows that both the imaginary and real parts of the refractive index are positive in the selected temperature and frequency ranges. This means that InSb behaves as a dispersive and loss full dielectric material. The extinction coefficient decreases with increasing frequency but the refractive index increases in contrast. The refractive index (extinction coefficient) rises (reduces) very sharply up to $\sim$ 10 THz and then saturates. The variations are very slow at low temperatures but quit fast (exponentially) at high temperatures. The temperature increase results in increase of the plasma frequency and then reduction of the real part. However, a growth in the imaginary part is observed. But at frequencies of $\sim>$ 12 THz, both the coefficients

are almost independent of the temperature.

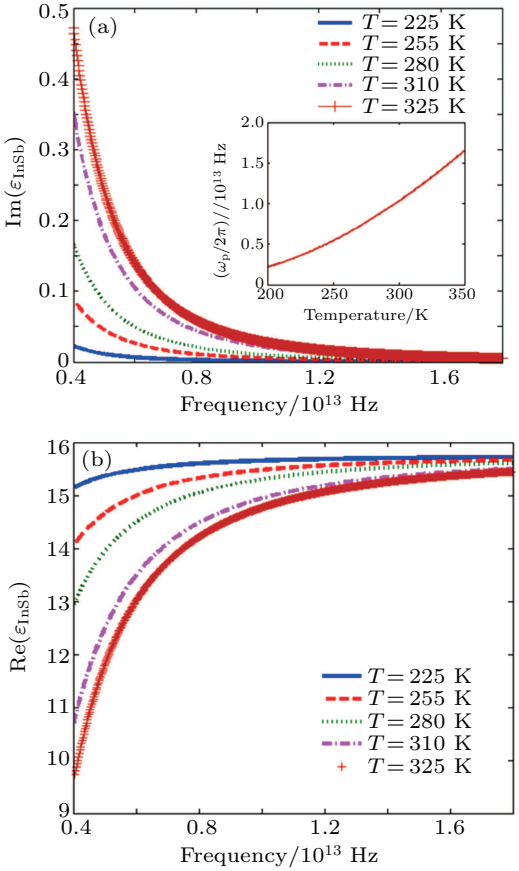


Fig. 7. Temperature dependence of the (a) real and (b) imaginary parts of the InSb dielectric permittivity. Inset in panel (a) shows the calculated plasma frequency of the InSb layer as a function of the crystal temperature.

Increase in the extinction coefficient results in more loss and thus the reduction of the crystal transparency. This is in consistence with the results presented in Figs. 5 and 6, which show that the intensities of the resonant modes reduce with temperature. Furthermore, as it was discussed above, the variation of the imaginary part is fast at lower frequencies, then it might be the cause for the smaller changes in the transmittance intensity of the high frequency modes by increasing the crystal temperature.

3.4. Incident angle dependence

Finally, the dependence of the optical features of the proposed defective crystals on the wave incidence angle is investigated by exploring the changes of these crystals' transmittances. Figures 8(a) and 8(b) are the color maps illustrating the variations of the transmittance versus frequency for different incident angles. It is worth noting that the angles are measured from normal. It is clear that as the incident angle increases, the PBGs size increases in both crystals. But the left hand side limits of the gaps are affected much less than the limit at the high frequencies. Furthermore, as a result, the defect layers' induced resonant modes shift to higher frequencies (blue shift). The behaviors are almost symmetric for the positive and negative angles. Thus besides of their temperature dependency, the optical response of the proposed defective crystals might be efficiently controlled by the crystal orientation respect to the wave propagation direction.

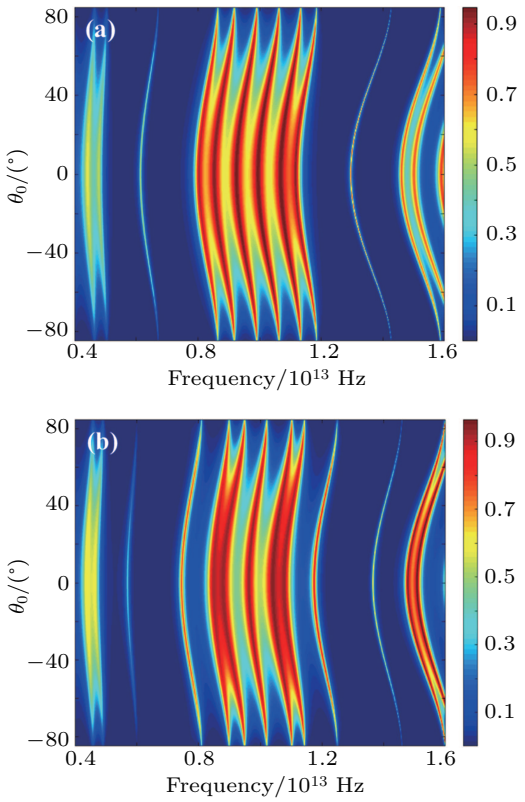


Fig. 8. Variations of the (a) FDPC and (b) SDPC transmittance versus frequency and the wave incident angle. Crystals' temperature is 300 K, $N_1 = 4$, $N_2 = 3$, and thicknesses of the SiO_2 and InSb layers are 4 μm.

In order to further discover the sensitivity to temperature and incident angle, the band gap widths are extracted and tabulated in Tables 1 and 2 for the FDPC and SDPC crystals, respectively. It is clear that at a fixed temperature, both gaps of the proposed structures have a same width at positive and negative values of an angle. However, at all the selected temperatures, deviation of the incident beam from normal (in positive/negative directions) results in an increase in the width of the gaps. Furthermore, similar to the normal incidence, at all positive/negative angles, the width of the gaps does not change considerably ($<\sim 2\%$) with increasing the crystal temperature. The only exception is the second gap of the SDPC structure for which an increase as high as $\sim 27\%$ is observed. However, the variation is not the same for all angles and with increasing the angle (from normal), the change of the PBG width gets less. In t other words, by raising the temperature from 225 K to 310 K, the largest amount of changes in PBG width belongs to the normal incidence ($\sim 27\%$). On the other hand, at $\theta = \pm 60^\circ$, the amount of change in the second gap of the SDPC structure is $\sim 23\%$.

Table 1. Width of the 1st and 2nd stop bands of the FDPC structure at various temperatures and incident angles.

Incident angle/(°)	Width of the 1st stop band			Width of the 2nd stop band		
	$T_1 = 225$	$T_2 = 285$	$T_3 = 310$	$T_1 = 225$	$T_2 = 285$	$T_3 = 310$
60	3.36	3.35	3.34	3.53	3.50	3.48
30	3.07	3.06	3.05	3.30	3.28	3.25
0	2.95	2.94	2.93	2.90	2.89	2.88
−30	3.07	3.06	3.05	3.30	3.28	3.25
−60	3.36	3.35	3.34	3.53	3.50	3.48

Table 2. Width of the 1st and 2nd stop bands of the SDPC structure at various temperatures and incident angles.

Incident angle/(°)	Width of the 1st stop band			Width of the 2nd stop band		
	$T_1 = 225$	$T_2 = 285$	$T_3 = 310$	$T_1 = 225$	$T_2 = 285$	$T_3 = 310$
60	3.78	3.77	3.75	4.19	3.25	3.23
30	3.51	3.51	3.50	3.74	2.92	2.75
0	3.42	3.4	3.4	3.56	2.79	2.60
−30	3.51	3.51	3.50	3.74	2.92	2.75
−60	3.78	3.77	3.75	4.19	3.25	3.23

4. Conclusion

One-dimensional ideal photonic crystal consisting of micrometer sized SiO_2/InSb alternating layers was proposed for terahertz applications. Optical response of two more defective structures (FDPC and SDPC), which are producible by disrupting the ideal crystal regularity, were also explored systematically besides the perfect PC. The results show that by changing the layers' thicknesses, a shift in the dispersion curve of the ideal crystal is observed. So that with increasing the thicknesses of the layers, the PBG intervals red shift and new gaps are generated at higher frequencies. The amount of changes is dependent on the amount of thickness changes. Inserting intentional defects in the crystal structure results in generation of the resonant mode(s) in the PBGs. Furthermore, the size of the gaps is also increased (compared to the ideal crystal) but the number of modes is different for the FDPC and SDPC. The width, central frequency, and the number of the PBGs of both defective crystals are seriously dependent on the thicknesses of the layers. In the case that the layers' thicknesses are the same, alterations of the crystals transmittance with the thicknesses of the unit cells are more predictable. In other words, the PBG intervals experience red shifts with rising the thicknesses of the layers and the central frequency of the defect layer(s) induced resonant modes also shifts continuously to the lower frequencies as a result. A blue shift in the total spectra of both the FDPC and SDPC structures is observed with increase in temperature and as a result defect modes shift to higher frequencies and their height (intensity) reduces. The central frequencies of all the modes are tunable with temperature. However, the dependence of different modes on temperature is different and the modes at lower frequencies are affected to some extent more. Both the proposed defective structures have a considerable response at temperatures as high as 300 K. Furthermore, the optical response of the crystals might be well controlled by adjusting the crystal orientation respect to the wave propagation direction. So that at entire of the selected temperatures, deviation of the incident beam from normal (in positive/negative directions) results in an increase in the width of the gaps. However, at large angles, temperature dependent changes of the PBG width become samller. In other words, as the temperature changes in the range of 225–310 K, the largest amount of variations ($\sim 27\%$) in PBG width belongs to the case that the light incidence is normal.

The followings are the advantages/excellences of the proposed structures: (i) optical response in terahertz frequency range, (ii) being made of common semiconductor and dielectric materials (not including materials such as graphene layers which are hard to be purely synthesized), (iii) reasonable layer thicknesses (in micrometer range, which is much easier to be fabricated compared to the nanometer sizes), (iv) low numbers of layers, (v) response in a wide range of incident angles and presenting almost omnidirectional band gaps, (vi) easy and effective tunability of the optical responses, (vii) good performance at high temperatures without additional cooling systems. Thus it seems clearly that these crystals might be affordable for terahertz technology in practice.

References

[1] Hosseini Motlagh N S, Parvin P, Ghasemi F, Atyabi F, Jelvani S and Abolhosseini S 2016 *Laser Phys. Lett.* **13** 075604

[2] Ghasemi F, Parvin P, Hosseini Motlagh N S and Abachi S 2017 *Biomed. Optics Express* **8** 512

[3] Razi S and Ghasemi F 2018 *Eur. Phys. J. Plus* **133** 49

[4] Ghasemi F, Razi S and Madanipour K 2018 *J. Electron. Mater.* **47** 2871

[5] El-Amassi D M, Taya S A, Ramanujam N R, Vigneswaran D and Udaiyakumar R 2018 *Superlattices Microstruct.* **120** 353

[6] Yablonovitch E 1987 *Phys. Rev. Lett.* **58** 2059

[7] John S 1987 *Phys. Rev. Lett.* **58** 2486

[8] Costa C H 2017 *Phys. Rev. B* **96** 125412

[9] Fu J, Chen W and Lv B 2016 *Phys. Let. A* **380** 1793

[10] Si J and Sun C 2017 *J. Appl. Phys.* **122** 133104

[11] Kriegel I and Scotognella F 2017 *Phys. E: Low-dimensional Syst. Nanostruct.* **85** 34
[12] Kriegel I and Scotognella F 2018 *Opt. Commun.* **410** 703
[13] Ghasemi F and Razi S 2019 *Laser Phys.* **29** 046204
[14] Amri R, Sahel S, Gamra D, Lejeune M and Bouchriha H 2018 *Opt. Mater.* **76** 222
[15] Liu C P and Fan T J 2014 *Opt. & Laser Technol.* **62** 82
[16] Zheng W 2018 *Chin. Phys. B* **27** 114211
[17] Nagaty A, Mehaney A and Aly A H 2018 *Chin. Phys. B* **27** 094301
[18] Wu J J, Li Sh G, Liu Q and Shi M 2017 *Chin. Phys. B* **26** 114209
[19] Zhang T, Sun J, Yang Y and Li Z 2018 *Opt. Commun.* **428** 53
[20] Lou J, Cheng T and Li S 2018 *Opt. Commun.* **426** 267
[21] Razi S and Ghasemi F 2019 *Opt. Quantum Electronics* **51** 1
[22] Ghasemi F, Roshan Entezar S and Razi S 2019 *Laser Phys.* **29** 056201
[23] Zhuang H, Kong F, Li K and Sheng S 2015 *Jpn. J. Appl. Phys.* **54** 095101
[24] Senn T, Bischoff J, Nüsse N, Schoengen M and Löchel B 2011 *Photon. Nanostruct.– Fundam. Appl.* **9** 248
[25] Wang F, Cheng Y Z, Wang X, Qi D and Luo H 2018 *Opt. Mater.* **75** 373e378
[26] Razi S, Varlamova O, Reif J, Bestehorn M and Ratzke M 2018 *Opt. & Laser Technol.* **104** 8
[27] Lee A J, Withford M J and Dawes J 2004 *PICALO* **2004** M103
[28] Ardakani A G, Kalantari T and Nadgaran H 2015 *Eur. Phys. J. B* **88** 241
[29] Brosi J, Koos Ch, Claudio Andreani L, Waldow M, Leuthold J and Freude W 2008 *Opt. Express* **16** 4177
[30] Segovia-Chaves F and Vinck-Posada H 2018 *Physica E* **104** 49
[31] Qi D, Cheng Y, Wang X, Wang F, Li B and Gong R 2017 *J. Phys. D: Appl. Phys.* **50** 505108
[32] Wang F, Cheng Y, Wang X, Zhang Y N, Nie Y and Gong R Z 2018 *Materials (Basel)* **11** 1099
[33] Qi D, Chen F, Wang X, Luo H, Cheng Y Z, Niu X Y and Gong R Z 2018 *Opt. Lett.* **43** 5323
[34] Razi S and Ghasemi F 2019 *Physica B* **566** 77
[35] Hung H C, Wu C J and Chang S J 2011 *J. Appl. Phys.* **110** 093110
[36] Qi L, Shang L and Zhang S 2014 *Phys. Plasmas* **21** 013501
[37] Qi L and Zhang X 2011 *J. Electromagn. Waves Appl.* **25** 539
[38] Dai X, Xiang Y, Wen S and He H 2011 *J. Appl. Phys.* **109** 053104
[39] Hu Z, Wu H, Gao S and Wang T 2012 *IEEE J. Quantum Electron.* **48** 1476
[40] Chang Y H , Jhu Y Y and Wu C J 2012 *J. Optoelectronics Advanced Materials* **14** 185
[41] Ghasemi F, Roshan Entezar S and Razi S 2019 *Phys. Lett. A* **383** 2551